Supplemental Document

optica

Optical phased array beam steering in the mid-infrared on an InP-based platform: supplement

JASON MIDKIFF,[1] KYOUNG MIN YOO,[1] JONG-DUG SHIN,[2] HAMED DALIR,[2] MOHAMMAD TEIMOURPOUR,[2] AND RAY T. CHEN[1,2,*]

[1] *Department of Electrical and Computer Engineering, University of Texas at Austin, Austin, Texas 78758, USA*
[2] *Omega Optics, Inc., Austin, Texas 78757, USA*
[*] *Corresponding author: chenrt@austin.utexas.edu*

Supplement DOI: https://doi.org/10.6084/m9.figshare.13054034

Parent Article DOI: https://doi.org/10.1364/OPTICA.400441

Optical phased array beam steering in the mid-infrared on an InP-based platform: supplemental material

Jason Midkiff,[1] Kyoung Min Yoo,[1] Jong-Dug Shin,[2] Hamed Dalir,[2] Mohammad Teimourpour,[2] and Ray T. Chen[1,2,*]

[1]*Department of Electrical and Computer Engineering, University of Texas at Austin, Austin, TX 78758, USA*

[2]*Omega Optics, Inc., Austin, TX 78757, USA*
**Corresponding author: chenrt@austin.utexas.edu*

Device Fabrication.

The updoped InP/InGaAs epitaxial layers were grown on an undoped InP substrate by MOCVD at OEpic Semiconductors, Inc. Fabrication on the epitaxial wafer began with a selective wet etch (HCl-based) of InP in the emitter region, leaving the InGaAs layer exposed. Next the phase shifter electrodes were formed by deposition and lift-off of Cr/Au (5nm/70nm). Then the emission gratings were patterned by e-beam lithography and dry etched 600 nm into the InGaAs layer by Cl_2/N_2 inductively coupled plasma reactive ion etch (ICP-RIE). Subsequently the waveguides were formed by $Cl_2/CH_4/H_2$ ICP-RIE, etching through the InP and InGaAs layers and into the InP substrate to a total depth of 5.5 μm. The waveguides were then passivated in the phase-shifter region with 2 μm SiO_2 (for 1 μm sidewall coverage), and contact openings to the electrodes were opened by CHF_3/Ar reactive ion etching. A sequence of Ti/Au (10nm/200nm) depositions (one normal and four oblique for continuous coverage across waveguide ridges) was carried out for creating the overlay from the contacts to the probe pads. Following device fabrication, the chip was cleaved at the input to allow end-fire coupling and affixed with indium to an aluminum carrier block for both electrical grounding and thermal heat sinking.

Phase shifting characterization.

A symmetric Mach-Zehnder interferometer was fabricated on the same chip as the OPA devices for phase shifting characterization. Fig. S1(a) shows the device. Laser, stage, lens and camera are the same as described below in "Beam steering test setup." Input light was end-fire coupled into the cleaved facet on one side of the chip, and the output light from another cleaved facet on the other side of the chip was viewed and measured with the mid-infrared camera (input and output facets were offset to avoid stray input light blinding the output). One arm of the MZI was biased by a contact probe and the substrate was grounded. The optical output vs. input electrical power is shown in Fig. S1(b), from which we estimate π-phase-shift to occur at ~225 mW electrical power.

The device suffered from parasitic resistances. In our design, ideally, the main resistance is through the undoped waveguide ridge. However, our particular substrate was also undoped, adding a resistance of ~2x that of the ridge; and at the time of fabrication we were not equipped to remove the substrate. The contact resistance between metal and ridge is another parasitic resistance, this one comparable in size to the ridge resistance. In effect, a straightforward analysis of the structure based on the undoped carrier concentration $n \approx 1\text{x}10^{15}$ cm^{-3}, yields values of 14, 17, and 31 Ω for the contact, ridge, and substrate resistances, respectively. However, these values assume an even distribution of current across the waveguide, which experiment showed not to be the case (due to a contact metallization that turned out to be thin and patchy). Having measured a total resistance of ~250 Ω, we estimate that the current distribution was limited to ~25% of the waveguide. Taking this factor into account, the three resistances become 56, 69, and 125 Ω. Moreover, the limited current distribution permitted greater heat dissipation through the metal overlay, thereby limiting the temperature increase in the waveguide. Hence, both the parasitic resistances and the facilitated heat dissipation through the metal are significant factors contributing the value of the π-phase-shift power, and we expect that a reduction of these factors could yield up to an order of magnitude reduction in the phase shifting power.

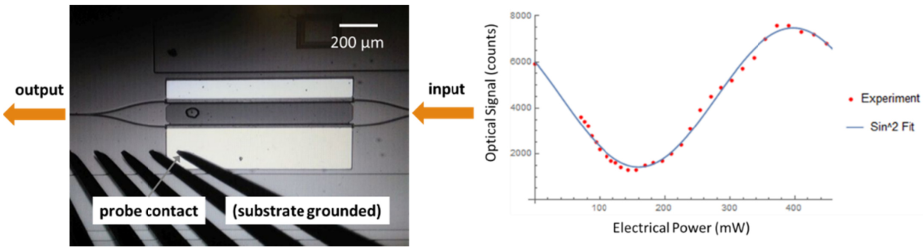

Fig. S1. Phase-shifter characterization with a Mach-Zehnder interferometer. (a) Microscope photo of the device with bias probe. (b) Plot of the optical output vs input electrical power.

Beam steering test setup.

The OPA chip, mounted on an Aluminum carrier block, was affixed to a Peltier cooling module (to withdraw the generated heat and maintain the chip at 21±2 °C) and positioned with a motorized stage (Newport). The quantum cascade laser (Adtech Optics) was focused onto the device's cleaved facet with a ½" diameter CaF_2 bi-convex lens of focal length = 16 mm at λ = 4.6 µm (Thorlabs). Laser output power was ~12 mW. Assuming a Gaussian beam profile with FWHM of ~30 µm, an input waveguide width of 20 µm, and a Fresnel reflection of 28%, the input power to the waveguide was calculated as ~0.6 mW. Two multi-contact probes (FormFactor DCQ-16), with 16 independent probe tips each, were used for contacting the 32 probe pads, as shown in Fig. 3(c). Five to seven power supplies were connected directly to the probe contact wires, running some connections in parallel for voltage distribution as needed. The flat paper screen was mounted 12 cm above the chip surface and the beam was observed on the screen with a mid-infrared (3-5 µm) camera (FLIR A6752sc).

Comparisons with other material platforms.

As discussed in the main text, the main advantage of a beam steerer fabricated on an InP-based platform is its potential for monolithic integration with high power QCLs, where reliability from thermal mismatch could be an issue with other (hybrid) systems. Apart from this benefit, there are other pros and cons associated with the choice of material system.

In comparison to waveguide/cladding systems of higher-index-contrast, the use of the low-index-contrast InGaAs/InP system will typically necessitate larger electrical steering power (and associated heat production) during the steering process (though further investigations and optimizations of phase shifting technologies are needed to fully assess the situation).

However, the lower-index-contrast is expected to permit operation to higher optical powers, since the modal profile can extend further into the cladding. To quantify the effect, we employ the mode's effective area A_{eff}, which provides a measure of the spreading of mode's energy. Table S1 presents a comparison of effective modal areas of our system with two other prominent mid-IR systems—Si/SiN and Ge/Si. The values were obtained from a mode solver (Lumerical) of ridge waveguides of equal cross-sectional areas (A = 1.8 x 1.8 μm^2). The mode profiles are shown in Fig. S2. For InGaAs/InP, in comparison to the other two systems, the results indicate ~20% greater modal spread, i.e. the approximate gain in optical power handling.

Table S1: Effective modal areas of selected material systems.

	InGaAs/InP	Si/SiN	Ge/Si
n @ λ=4.6μm	3.42/3.09	3.42/2.36	3.98/3.42
A_{eff} (μm^2)	3.16	2.63	2.50
A_{eff}/A	0.98	0.81	0.77

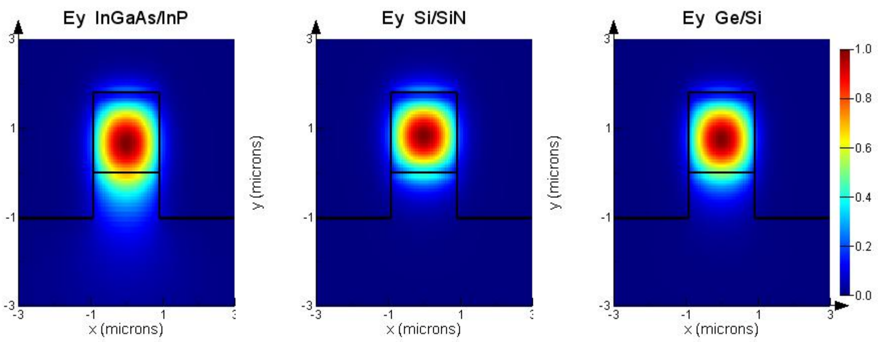

Fig. S2. Simulated fundamental TM mode profiles for three core/cladding material systems: InGaAs/InP, Si/SiN, Ge/Si. The same dimensions are employed for each case: core 1.8 x 1.8 μm^2, sub-cladding 1.8 x 1.0 μm^2.

In regards to lateral steering range, InGaAs waveguides can be expected to perform on par with Si waveguides, since the channel pitch is dictated by the horizontal index contrast, which when the waveguides are separated by air will be similar for both cases since their indices are nearly equal. In contrast, Ge waveguides will have an advantage here with their higher index.

Comparisons with other non-mechanical beam steerers in the 3–5 μm spectral window.

Table S2 presents a comparison of our non-mechanical beam steerer with other selected demonstrations in the 3–5 μm spectral window. Each has its pros and cons, and generally, as the technologies mature, each one may be appropriate for a certain application. The diffractive waveplate and FT-OPO-based devices will likely be limited to bulk optics. The SEEOR may see use in a component-packaged device. The Ge/Si OPA may lead to hybrid integration with low power sources. And finally, reiterating, our InP-based OPA is the only one with potential for integration with high power QCL sources.

Table S2: Non-mechanical beam steerers in the 3–5 μm spectral window.

Technology	System	Steering Range	Resolvable points	Electrical Steering energy	Optical Insertion Loss	Response time[a]	Ref.
Diffractive waveplate	LC (UCF-M3)	7.6°	2	V_{drive} = 80 V_{rms}	0.1 dB	~s	[1]
AO cell FT-OPO	TeO_2 AO scanner, KTA crystal	2° x 2°	46 x 46	P_{RF} = 2 W[b]	16 dB	~μs	[2]
SEEOR	LC (custom)/As_2Se_3/As_2S_3/Si	14° x 0.6°	28 x 2	V_{drive} up to 500 V	15 dB	n.d.	[3]
12-channel OPA	Ge/Si	45° x 12°	15 x 67	P_π = 52 mW	n.d.	~ms	[4]
32-channel OPA	InGaAs/InP	23° x 9°	38 x 15	P_π = 225 mW	18 dB	~ms	this work

[a] estimates based on steering technology, [b] from AO cell specification sheet, LC = Liquid Crystal, AO = Acousto-Optic, FT-OPO = Fourier Transform Optical Parametric Oscillator, SEEOR = Steerable ElectroEvanescent Optical Refractor, n.d. = no data or unknown

References

1. F. Gou, F. Peng, Q. Ru, Y.-H. Lee, H. Chen, Z. He, T. Zhan, K. L. Vodopyanov, and S.-T. Wu, Opt. Express 25, 22404 (2017).
2. J. Bourderionnet, A. Brignon, D. Dolfi, and J.-P. Huignard, Adv. Opt. Techn. 6, 103 (2017).
3. J. A. Frantz, J. D. Myers, R. Y. Bekele, C. M. Spillman, J. Naciri, J. Kolacz, H. G. Gotjen, V. Q. Nguyen, C. C. McClain, L. B. Shaw, and J. S. Sanghera, J. Opt. Soc. Am. B 35, C29 (2018).
4. M. Prost, Y.-C. Ling, S. Cakmakyapan, Y. Zhang, K. Zhang, J. Hu, Y. Hu, Y. Zhang, and S. J. B. Yoo, IEEE Photonics J. 11, 6603909 (2019).